Journal of Hydrology 592 (2021) 125841

Contents lists available at ScienceDirect

Journal of Hydrology

journal homepage: www.elsevier.com/locate/jhydrol

Research papers

The transport mechanism of carbon isotopes based on 10 years of cave monitoring: Implications for paleoclimate reconstruction

Yidong Li [a], Yan Yang [a,*], Xiuyang Jiang [b], Jingyao Zhao [c], Zhe Sun [d], Xiao Shi [a], Ning Tian [a], Yunyue Yang [b], Jiancang Li [e], Junwei Duan [e]

[a] Chongqing Key Laboratory of Karst Environment & School of Geographical Sciences, Southwest University, Chongqing 400715, China
[b] Institute of Geography, Fujian Normal University, Fuzhou 350007, China
[c] Institute of Global Environmental Change, Xi'an Jiaotong University, Xi'an 710054, China
[d] Key Laboratory of Alpine Ecology, Institute of Tibetan Plateau Research, Chinese Academy of Sciences, Beijing 100101, China
[e] Henan Jiguan Cave Tourism Development Limited, Luanchuan 471500, China

ARTICLE INFO

This manuscript was handled by Corrado Corradini, Editor-in-Chief, with the assistance of Yongjun Jiang, Associate Editor

Keywords:
Carbon isotopes
Karst hydrology
El Niño Southern Oscillation
Extreme drought events
Modern speleothems

ABSTRACT

Cave monitoring is crucial to unraveling the factors controlling carbon isotope compositions and their transportation in karst systems. Here, we report a 10-year (2010 ~ 2019) cave monitoring of carbon isotopes from the plants, soil, cave water, and speleothems in Jiguan Cave, Central China, located on the Chinese north–south divide in an area that is sensitive to the Asian monsoon. The results show that the cave ventilation and soil air CO_2 controlled by the local temperature and humidity conditions are responsible for the seasonal variability in the $\delta^{13}C_{DIC}$ values. The variation in the $\delta^{13}C_{DIC}$ values and trace element ratios of the cave water are sensitive to the local hydrological conditions. Although there is the lag time from precipitation to cave water in drought year, the $\delta^{13}C_{DIC}$ and trace element ratios (Mg/Ca, Ba/Ca and Sr/Ca) of cave water are strongly coupled and reflect the extreme drought due to the influence of prior calcite precipitation (PCP) and water–rock interaction. The 10-year monitoring period covered two complete El Niño Southern Oscillation (ENSO) cycles. During the two strong El Niño years (2010 and 2015), the cave drip water $\delta^{13}C_{DIC}$ values were negative but the $\delta^{18}O$ values were positive. This opposite trend is mainly due to their different controlling mechanisms. The rainfall amount and moisture sources are responsible for the $\delta^{13}C_{DIC}$ and $\delta^{18}O$ values of the drip water, respectively. Throughout the karst cave system, the carbon isotopes in Jiguan Cave are continuously enriched when migrating from the vegetation to the soil to the cave drip water to the modern speleothems. Comparisons with the stalagmite $\delta^{13}C$ records for the nearby Jiguan Cave suggest that stalagmite carbon isotopes may reflect the regional precipitation changes induced by the ENSO on the decadal scale. Overall, we demonstrate that the $\delta^{13}C$ is a potentially reliable proxy that records the changes in the regional environment, especially precipitation changes, and is also a sensitive indictor that indirectly reflects ENSO.

1. Introduction

Cave speleothems formed by water–rock interactions are a rare and important source of information for the study of paleoclimate evolution in karst areas (Wang et al., 2001; Shopov et al., 2004; Yuan et al., 2004; Banner et al., 2007; Cheng et al., 2009, 2016; Cai et al., 2010). The stalagmite $\delta^{18}O$ is the most widely used environmental proxy and has been extensively used to reconstruct paleoclimates (Yuan et al., 2004; Cobb et al., 2007; Tan et al., 2009, 2018, 2020a, 2020b; Pausata et al., 2011; Maher and Thompson, 2012; Tan, 2014; Zhao et al., 2019; Liu et al., 2020). Nevertheless, the interpretation of stalagmite $\delta^{18}O$ is still debated. In general, previous interpretations of speleothem $\delta^{18}O$ have primarily focused on the rainfall amount effect (Hu et al., 2008; Zhang et al., 2008; Goldsmith et al., 2017), temperature effect (Paulsen et al., 2003; Feng et al., 2014), monsoon intensity (Yuan et al., 2004; Wang et al., 2005; Cheng et al., 2016), moisture source change (Cobb et al., 2007; Maher, 2008; Maher and Thompson, 2012), and circulation effect (Tan, 2014, 2016, Sun et al., 2018).

Although stalagmite $\delta^{13}C$ are not as widely used as $\delta^{18}O$, previous studies suggested that carbon isotopes are more sensitive to changes in

* Corresponding author at: NO. 2 Tiansheng Road, Beibei District, Chongqing 400715, China.
E-mail address: yy2954@swu.edu.cn (Y. Yang).

https://doi.org/10.1016/j.jhydrol.2020.125841

the local climate and ecological environment than oxygen isotopes (Frappier, 2013; Li et al., 2020), and the $\delta^{13}C$ time-series can be used as a valuable supplement to $\delta^{18}O$ compositions (Lambert and Aharon, 2011; Lechleitner et al., 2017). Many scholars have discussed the climate and environment information recorded by carbon isotopes (Fairchild et al., 2000; Tan et al., 2013; Li et al., 2020; Wu et al., 2020) and used $\delta^{13}C$ as an important proxy in paleoclimate and paleoenvironment reconstruction (Dorale et al., 1992; Coplen et al., 1994; Bar-Matthews et al., 1999; Genty et al., 2003; Woo et al., 2015; Zhang et al., 2015; Liu et al., 2016; Tan et al., 2020a, 2020b). However, the migration process of $\delta^{13}C$ signals in the entire cave system is affected by diverse complex factors, including climatic and non-climatic factors, which pose a significant challenge in explaining and interpreting the carbon isotope compositions of stalagmites. The types and density of vegetation overlying the cave and soil respiration rate affect the $\delta^{13}C$ of soil air CO_2 and indirectly reflect the changes of external climatic conditions (Cerling, 1984; Bar-Matthews et al., 1997; Dorale et al., 1998; McDermott, 2004; Fleitmann et al., 2009). Speleothem $\delta^{13}C$ values are also influenced by the inorganic processes operating in the soil zone, deeper within the unsaturated zone, and during calcite reprecipitation in the cave (Cosford et al., 2009). The degree of open versus closed system dissolution of the carbonate bedrock affects speleothem $\delta^{13}C$ values by controlling the proportions of carbon from different sources (Hendy, 1971; Genty et al., 2003; Fairchild et al., 2006a; Rudzka et al., 2011). In addition, prior carbonate precipitation (PCP) in the vadose zone cave ventilation, and the degassing of CO_2 from the drip water, also influence the final $\delta^{13}C$ values recorded in the speleothems (Baker et al., 1997; Verheyden et al., 2000; Spötl et al., 2005; Fairchild et al., 2006a; Baldini et al., 2008; Pu et al., 2017). Due to the complexity of the above factors, the application of speleothem $\delta^{13}C$ to reconstruct environmental changes has been limited.

The hydrological information provided by the trace element compositions of the cave water is an important proxy for reconstructing climate changes (Fairchild and Treble, 2009; Chen and Li, 2018; Zhang and Li, 2019). Multiple mechanisms control the trace elements composition of drip water, including the composition of the local soil and bedrock, the types of flow paths, the residence time of underground water, water–rock interaction, the extent and intensity of PCP, incongruent calcite dissolution, and the mixing of old and fresh water (Tooth and Fairchild, 2003; Fairchild and Treble, 2009; Sherwin and Baldini, 2011; Wong et al., 2011). These factors, which may affect the trace element ratios of drip water, have direct or indirect links to the precipitation (Zhang and Li, 2019). The combination of carbon isotope and trace element compositions can be used to rule out several possible mechanisms for the changes in stalagmite $\delta^{13}C$ (Hellstrom and McCulloch, 2000; McDermott, 2004; Zhang et al., 2015). Moreover, applying a multi-proxy approach such as $\delta^{18}O$ and trace elements can better constrain speleothem $\delta^{13}C$ variability and shed light on the dominant processes that influence $\delta^{13}C$ variability in a given cave system (Oster et al., 2010; Fohlmeister et al., 2017, 2020).

Cave monitoring can provide the opportunity to explore the transmission processes of $\delta^{13}C$ signals and quantify the effects of the seasonal and multi-year changes in the cave environment on the $\delta^{13}C$ record, and finally to evaluate the roles of various factors on speleothem $\delta^{13}C$ values (Genty and Massault, 1999; Baker and Brunsdon, 2003; Spötl et al., 2005; Fairchild et al., 2006a; Fuller et al., 2008; Lambert and Aharon, 2011). In this study, a 10-year monitoring program (2010–2019) was conducted in Jiguan cave, which is located in an area of Central China that is sensitive to variations in the Asian monsoon and the Western Pacific Subtropical High (WPSH). Previous monitoring results have shown that the interannual $\delta^{18}O$ of precipitation correspond to the variations in the El Niño Southern Oscillation (ENSO), which supports the interpretation of the circulation effect (Sun et al., 2018). Zhao et al. (2019) found that the changes in the $\delta^{18}O$ values of drip water and modern calcite are correlated with the shifts of WPSH, and they used a high-resolution $\delta^{18}O$ record from Dongshiya Cave, which is near Jiguan Cave, to reconstruct the variations of the WPSH western boundary. However, interpretations of the carbon isotope in cave system are rarely reported. Here, we present a 10-year study on carbon isotope and trace element compositions of the Jiguan cave system, and compare with the high-resolution $\delta^{13}C$ speleothem (DSY-1201) record that reported in Dongshiya Cave (Zhao et al., 2019). This study mainly focuses on the following questions: (1) the factors affecting the carbon isotope records in karst cave on different time scales (e.g., seasonal, annual and decadal); (2) the responses of trace elements ratios and carbon isotopes in cave water to the external environment; (3) the responses of karst hydrology $\delta^{13}C$ values to ENSO, and their implications for the use of $\delta^{13}C$ records in paleoclimate reconstruction.

2. Study area

Jiguan Cave (33°46′ N, 111°34′ E) and Dongshiya Cave are located in the north slope of Funiu Mountain, which is approximately 4 km southwest of Luanchuan County, Henan Province, Central China (Fig. 1a and b). The two caves are about 300 m away from each other (Zhao et al., 2019). The site is located in the northern part of the Qinling Mountains-Huaihe River Line in the northern part of the Yangtze River and Yellow River watershed. The study area is in the transition zone between the humid region and the semiarid region, and it is sensitive to the Asian summer monsoon. The mean annual temperature and precipitation recorded at the meteorological station in Luanchuan were 12.4 °C and 838 mm (1957–2019), respectively (Supplementary Table S1). Owing to the influence of the monsoon, more than 50% of the annual precipitation is concentrated in summer. The overlying bedrock is relatively thin and mainly consists of Sinian chloritization marble with a thickness of 30–40 m (Fig. 2). The surface vegetation has mainly been a secondary deciduous broad-leaved forest since about 1993. The soil overlying the mountain is brown soil with a thickness of 10–60 cm.

The elevation of the entrance of Jiguan Cave is approximately 900 m, the length is approximately 5600 m, and one-third of the cave has been developed for tourism (Sun et al., 2018). During the monitoring period, the temperature in the cave ranged from 13.5 ℃ to 17.0 ℃ (averaged of 15.5 ℃), and the relative humidity was remained higher than 90% all year round, indicating that the internal environment of Jiguan Cave is relatively closed.

3. Sample collection and data analysis

3.1. Sample collection

Soil profile was excavated at altitudes of 900–920 m from the roof of Jiguan Cave (Fig. 1c). To avoid potential cross-contamination of the subsamples of soil profile, the soil subsamples were collected from bottom to top at intervals of 5 cm. Leaf, branch, and root samples were collected from the dominant plants near each soil section.

Five cave water sampling sites were monitored in Jiguan Cave (Fig. 1d), including one underground river (DTH: Dong Tian He), two drip water sites (LYXS: Li Yu Xi Shui and TGBD: Tian Gong Bing Deng), and two pool sites (YZT: Yu Zhu Tan and YCG: Yao Chi Gong). The polypropylene bottles that were used to collect the water samples were rinsed in 1:1 HCl and deionized water prior to the sample collection. Prewashed 0.45 μm Millipore nitrocellulose filters were used to filter the water samples before the samples were added to the sample bottles. A pre-cleaned container (not acid washed) was left for 1–3 h to collect the drip water, and then, aliquots were poured into acid-cleaned polypropylene sample bottles. The trace level ultrapure HNO_3 (1:1) was added to achieve the pH value of <2 for cation samples. To avoid isotope fractionation caused by microorganisms, 0.2 mL of saturated $HgCl_2$ solution was added to the dissolved inorganic carbon (DIC) samples. All of the samples were sealed, transported to the laboratory, and stored at 4 °C until analyzed. The cave water sites were sampled at two month intervals starting in 2010 and at one month intervals starting in April

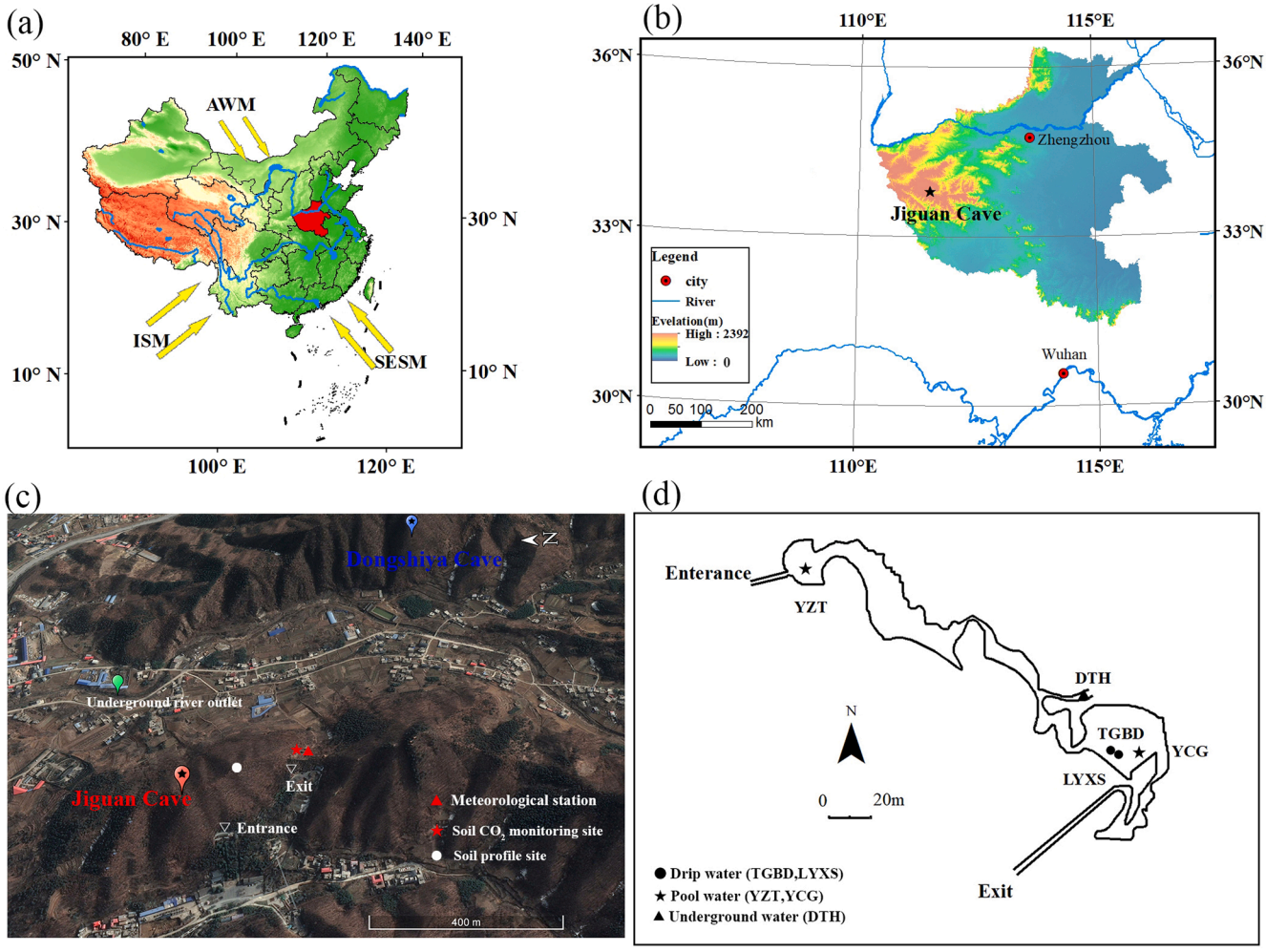

Fig. 1. (a) Location of study area, Jiguan cave in central China. Yellow arrows indicate the Asian Winter Monsoon (AWM), the Indian Summer Monsoon (ISM) and the Southeast Summer Monsoon (SESM). (b) Location of Jiguan cave (black star) in Henan province. (c) The topographic map of Jiguan cave. The white triangle is the entrance and exit, the red triangle and star represent the meteorological station and soil CO_2 monitoring site, respectively. The base map is derived from Google Earth. (d) Distribution of monitoring sites in Jiguan cave. YZT (Yu Zhu Tan) and YCG (Yao Chi Gong) are pools, LYXS (Li Yu Xi Shui) and TGBD (Tian Gong Bing Deng) are drips, DTH (Dong Tian He) is underground river in the cave (modified after Sun et al.,2018). (For interpretation of the references to colour in this figure legend, the reader is referred to the web version of this article.)

2019.

Two circular glass plates were placed under the drip sites to collect modern deposits. The glass plates were replaced every two months and were dried naturally at room temperature after being rinsed with deionized water. Powder subsamples were scraped from the modern sediment sample on the glass plate using a clean steel knife. If no deposits were found, the retrieval was temporarily paused.

3.2. Sample analyses

The methods used to measure the oxygen isotopes of the water samples (2009–2016) have been described by Sun et al. (2018). The samples collected from 2017 to 2019 were analyzed using the Picarro L2140-iCRDS liquid water isotope analyzer at the Stable Isotope Laboratory, School of Geographical Sciences, Fujian Normal University. The measurement accuracy was typically ±0.08‰ and the results (Supplementary Table S2) are reported relative to V-SMOW (Vienna Standard Mean Ocean Water). The $\delta^{13}C_{DIC}$ analyses were conducted in the Chongqing Key Laboratory of Karst Environments at Southwest University and in the Isotope Laboratory of the Institute of Karst Geology, Chinese Academy of Geological Sciences. The analyses were performed using a Delta-V-Plus mass spectrometer connected to a gas bench pre-treatment apparatus. The analysis precision was better than 0.2% (1σ).

The $\delta^{18}O$ and $\delta^{13}C$ values of the modern speleothems (Supplementary Table S3) were measured using a Finnigan Delta-V-Plus gas isotope mass spectrometer combined with a Kiel IV automated carbonate device. Each sample was analyzed 8 times, and the long-term 1σ precision is 0.1‰ for $\delta^{18}O$ and 0.06‰ for $\delta^{13}C$. The methods used to measure the carbon isotopes of the plant and soil organic matter have been described by Li et al. (2012). The analyses were conducted in the Geochemistry and Isotope Laboratory at Southwest University. All of the carbon isotopic results (Supplementary Table S4) obtained in this study are reported relative to V-PDB (Vienna Pee Dee Belemnite).

The Ca, Ba, Sr and Mg concentrations of the samples were measured using an Optima-2100DV inductively coupled plasma optical emission spectrometer (USA) in the Chongqing Key Laboratory of Karst Environments at Southwest University. The detection limit was 0.001 $mg{\cdot}L^{-1}$, and the relative uncertainty of the measurements is less than 2%. The data is presented in Supplementary Table S5.

3.3. Cave monitoring and meteorological data

We installed CO_2-monitoring devices between the bedrock and soil on the southern slope above Jiguan Cave in May 2019 (Fig. 1c). The

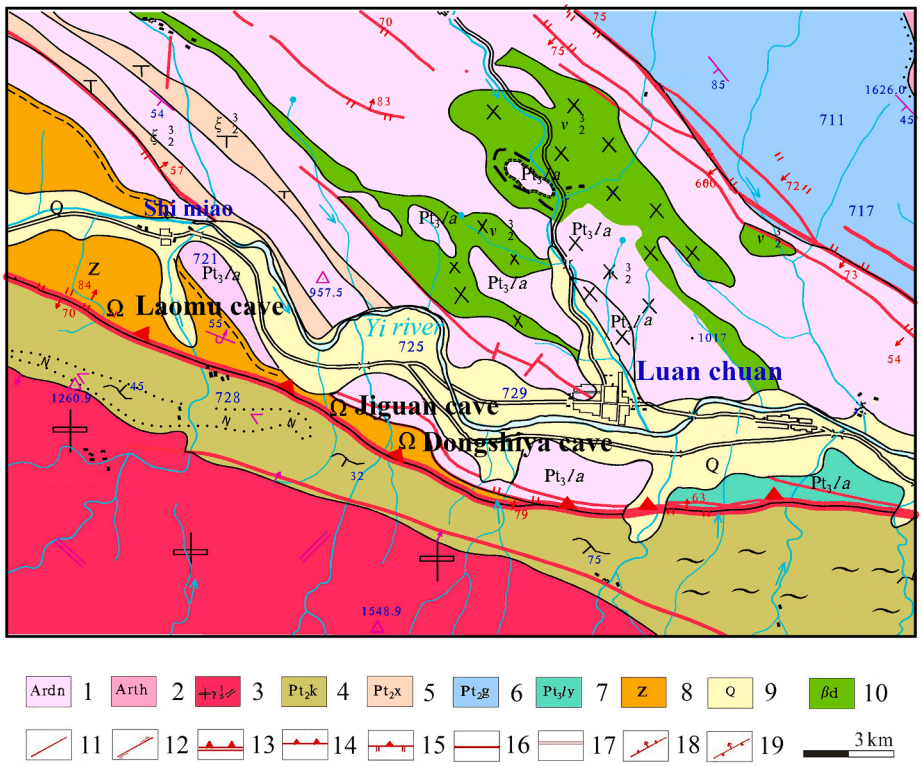

Fig. 2. Location distribution and regional geological map of Jiguan cave. The base map is derived from Regional geological map of Luanchuan, Henan Province. 1. the Archean Dengfeng Group; 2. the Archean Taihua Group; 3. granite porphyry in the late Indosinian-yanshanian period; 4. Kuanping Group of the middle Proterozoic erathem; 5. Xionger Group of the middle Proterozoic erathem; 6. Guandaokou Group of the middle Proterozoic erathem; 7. Luoyu Group of the Neoproterozoic erathem; 8. Sinian system; 9. Quaternary system; 10. Daan Basalt; 11. fault of unknown nature; 12. blatt fault and Strike-Slip Fault; 13. the lithospheric fracture of the geosuture; 14. lithospheric fault; 15. thrust fault; 16. basement fault; 17. caprock and surface fracture; 18. normal fault; 19. reverse fault.

ranges of the GMM221 soil CO_2 concentration sensor (Vaisala, Finland), the Av-10T soil temperature sensor (USA), and the Av-EC5 soil moisture sensor are 0–20000 $\times 10^{-6}$, 40 ℃–140 ℃, 0%–100%, respectively, with precisions of ±1%, ± 0.1℃ and ±0.1%, respectively. A TESTO 535 infrared CO_2 tester produced in Germany with range of 0–9999 ppmv was used to monitor the cave air CO_2 at five monitoring sites. The soil air pCO_2 and cave air pCO_2 data are presented in Supplementary Tables S6 and S7, respectively.

The temperature and precipitation data (Supplementary Table S1) collected before April 2019 were obtained from the meteorological station in Luanchuan County, Henan Province. In April 2019, a Vantage Pro field meteorological station produced by Davis was installed near the soil monitoring site to automatically log the temperature and precipitation data every 15 min, with precisions of 0.1 ℃ and 0.01 mm, respectively (Fig. 1c). The precipitation anomaly percentage was used to classify the extremely dry and wet years, the calculation formula is as follows:

$$P_a = (P - \overline{P})/P \times 100\%$$

where P_a is the percentage of precipitation anomaly, P is the annual precipitation in a year, and $\overline{P}$ is the average multi-year precipitation. Generally, the wet and dry years are distinguished by P_a values of 15% and −15%, respectively. In particular, a year with a P_a value of less than or equal to −40% was defined as an extremely drought year, and that with the P_a value of greater than or equal to 40% was defined as an extremely wet year (Wei et al., 2017).

The Niño 3.4 sea surface temperature anomaly (SSTA) data (http://www.cpc.ncep.noaa.gov/data/indices/sstoi.indices) were downloaded from the climate prediction center of the National Oceanic and Atmospheric Administration.

4. Results

4.1. Local temperature and precipitation

As is showed in Fig. 3d, the monthly mean temperature data varied with season. It was lower in winter (mean T = 1.8 ± 1.0 ℃) and higher in summer (mean T = 23.3 ± 1.5 ℃). All of ± in this paper represent the standard deviations. The local precipitation exhibited obvious seasonal changes and was mainly concentrated in the summer. However, the highest monthly precipitation occurred in different months each year. The total annual precipitation reached its peak (1105 mm) in 2010, and then, it gradually decreased, reaching its lowest point (435 mm) in 2013. The total amount of precipitation gradually increased from 2013 to 2015, and then, it decreased after 2015.

According to the 10-year percentage of precipitation anomaly (Supplementary Table S8), the P_a values in 2010, 2011, and 2015 were 50%, 29%, and 24%, respectively, thus these years were classified as wet years. The P_a values in 2013 and 2019 were −41% and −27%, respectively, thus they were classified as dry years. In particular, the P_a values in 2010 and 2013 were higher than 40% and lower than −40%, classifying them as extremely wet and extremely dry years, respectively. In 2010, the precipitation on July 24 alone was as high as 155 mm, this high rainfall event led to severe flooding in study area. From July 2013 to June 2014, the weather was extremely dry. The precipitation gradually increased after July 2014 and reached a peak of 242 mm in September. In the autumn of 2017, a relative severe drought event occurred. The precipitation was as high as 192 mm in September and sharply decreased to 62 mm in October (Fig. 3d).

We also analyzed the percentage of precipitation anomaly data (Supplementary Table S1) for the past 60 years, and found that the extremely wet years included 1964 (65%) and 1973 (43%), and the relatively wet years included 1967, 1983, 1984, 1996, 2005 and 2010. The dry years included 1966, 1969, 1972, 1976, 1978, 1986, 1991, 1997, 1999, 2012, and 2016 to 2019. Among them, 2013 (−48%) was an extremely drought year.

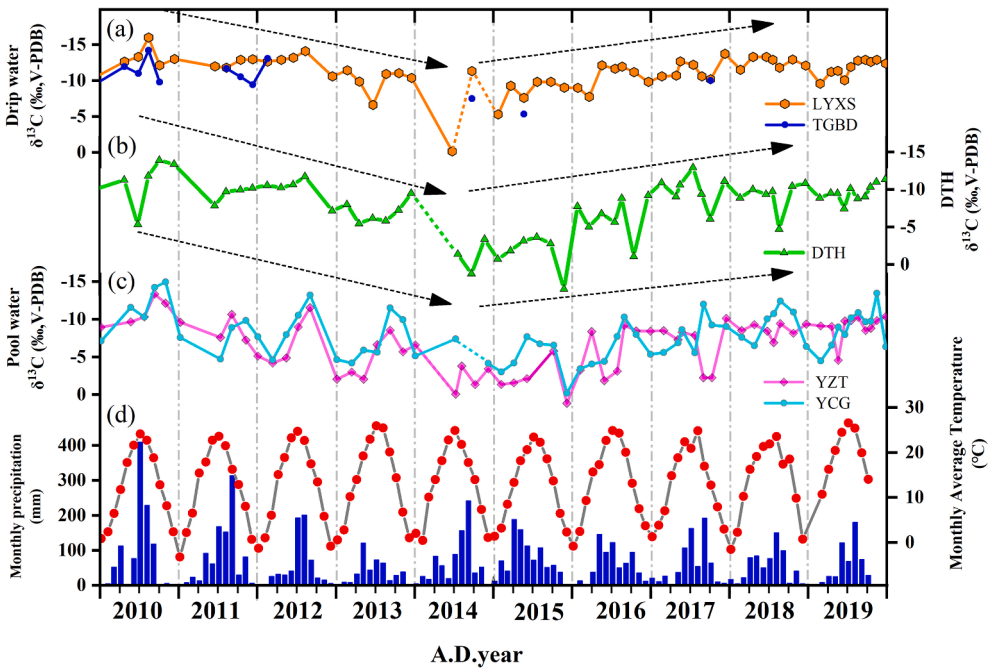

Fig. 3. (a) The variation of LYXS (orange polygon) and TGBD (blue dots) $\delta^{13}C_{DIC}$. (b) The variation of DTH (green triangle) $\delta^{13}C_{DIC}$. (c) The variation of YZT (nattier blue dots) and YCG (pink diamond) $\delta^{13}C_{DIC}$. (d) The monthly mean temperature (red dots) and amount of precipitation (blue histogram) out Jiguan cave during the monitoring period. The dotted line represents the trend of missing data, and the black dotted arrow represents the interannual variation trend of $\delta^{13}C_{DIC}$ of each monitoring site. (For interpretation of the references to colour in this figure legend, the reader is referred to the web version of this article.)

4.2. $\delta^{13}C_{DIC}$ values of cave water

The $\delta^{13}C_{DIC}$ values of the drip water, pool water, and the underground river are presented in Table 1. The $\delta^{13}C_{DIC}$ values of both drip sites and the pool sites exhibited seasonal variations, but the drip water $\delta^{13}C_{DIC}$ values exhibited more variable time-series than the pool water (Fig. 3a and c). The $\delta^{13}C_{DIC}$ values of the pool water exhibited clear seasonal signals, with summer/fall months having lower $\delta^{13}C_{DIC}$ values than the winter/early spring months when the $\delta^{13}C_{DIC}$ was substantially more ^{13}C-enriched (Fig. 3c). On the annual scale, the $\delta^{13}C_{DIC}$ values of the cave water were the most negative in 2010, and then, they gradually increased. The $\delta^{13}C_{DIC}$ values were the most positive in 2014, and then, they decreased (Fig. 3).

4.3. pCO_2 of the soil and cave air

The soil air pCO_2 overlying Jiguan Cave exhibited significant seasonal variations from May to December, with higher values in the summer and lower values in the winter. This variation pattern was quite consistent with that of the precipitation (Fig. 4b).

The cave air pCO_2 exhibited a significant seasonal variation pattern that was higher in the summer and lower in the winter (Fig. 4c). However, the pCO_2 of the four sites varied within different ranges. From 2017 to 2019, the pCO_2 of the four monitoring sites in the cave ranged from 347 ppmv to 1782 ppmv for YZT, 335 ppmv to 2503 ppmv for DTH, 429 ppmv to 4520 ppmv for YCG, and 462 ppmv to 4980 ppmv for LYXS, with averages of 743, 1028, 1727, and 2096 ppmv, respectively. The trends and amplitudes of the variations of drip water site LYXS and the nearby pool water site YCG were similar, and both were significantly higher than those of sites DTH and YZT (Fig. 4c).

4.4. The trace element compositions of cave water

The trace element compositions and ratios of the three types of cave water are summarized in Table 2. Mg/Ca values range from 0.29 to 0.50 mg/L; Sr/Ca values range from 0.85 to 2.36 mg/L; and Ba/Ca values range from 0.19 to 0.66 mg/L (Table 2). The Mg/Ca, Sr/Ca, and Ba/Ca values of the pool water and the underground river exhibited similar trends with obvious seasonal characteristics, i.e., higher values in the dry season and lower values in the rainy season. Although the trace element ratios of the drip water (LYXS) were relatively stable overall and did not exhibit seasonal variations, all three types of cave water showed significantly similar fluctuations in 2014 and 2017 (Fig. 5).

4.5. $\delta^{18}O$ values of the drip water and $\delta^{13}C$ values of the modern deposits, plants and soils

The $\delta^{18}O$ values of drip water fluctuated from −10.2‰ to −6.5‰. Although there was no seasonal variation in drip water $\delta^{18}O$, it showed dramatic changes with a rapid decrease of 3.55‰ from 2009 to 2010 and a rapid increase of 2.23‰ in 2015 (Fig. 6a).

The $\delta^{13}C$ values of modern speleothems ranged from −12.0‰ to −5.2‰ (average of -9.0 ± 1.7‰) for LYXS and from −9.0‰ to −12.5‰ (average of -10.9 ± 1.0‰) for TGBD. The modern speleothems $\delta^{13}C$ values exhibited seasonal variations in 2010 and 2011, negative in summer and positive in winter. The severe drought led to a hiatus in the depositional record in 2013, and carbonate recovered in November 2014 since drought was released by the increasing rainfall and drips were oversaturated for precipitation (Sun et al., 2017). Obviously, the variations in modern speleothem $\delta^{13}C$ values were synchronous with the $\delta^{18}O$ variations (Fig. 6d and e).

Table 1
$\delta^{13}C_{DIC}$ date for samples of cave water (V-PDB/‰).

	Min$\delta^{13}C_{DIC}$ (‰)	Max$\delta^{13}C_{DIC}$ (‰)	Mean$\delta^{13}C_{DIC}$ (‰)	Standard deviation (‰)	Sample number
YZT (pool)	−13.3	1.2	−6.8	3.4	64
YCG (pool)	−14.9	−0.2	−7.9	3.0	64
DTH (underground river)	−13.9	−0.7	−8.1	3.3	65
LYXS (drip)	−16.0	−0.2	−11.2	2.3	64
TGBD (drip)	−14.2	−5.3	−10.3	2.3	12

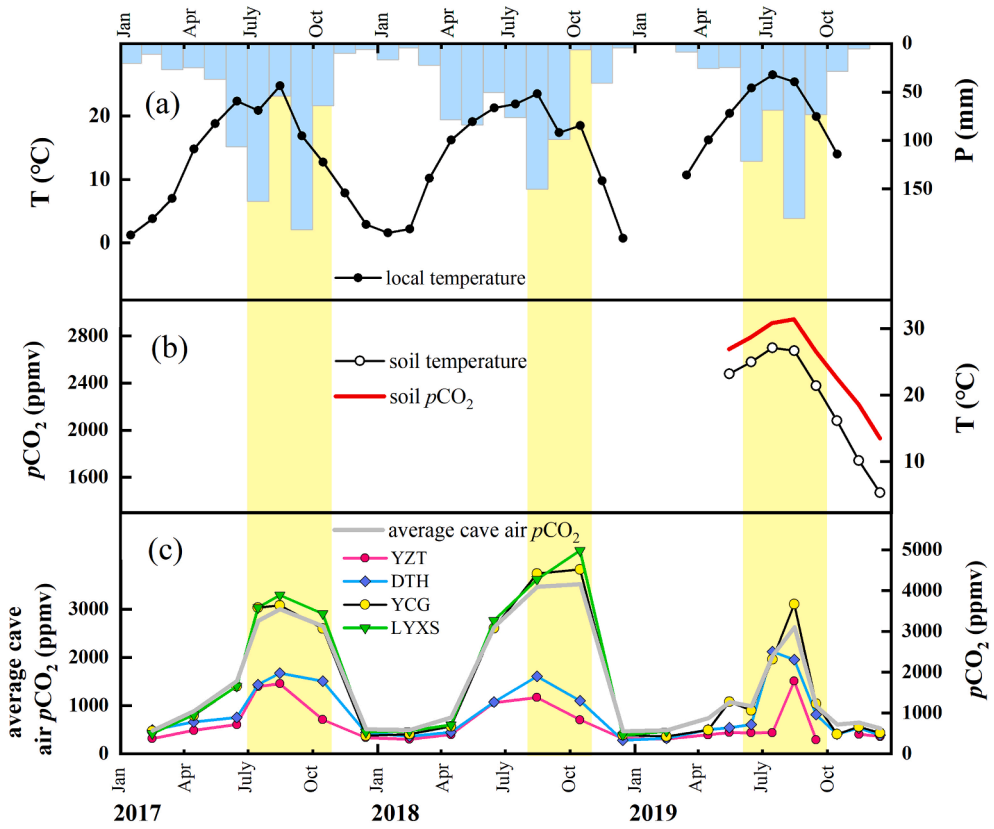

Fig. 4. (a) The variety of temperature and precipitation in the study area from 2017 to 2019. (b) The temperature and pCO_2 in soil overlying the cave in 2019. (c) Cave air pCO_2 for monitoring sites in the Jiguan cave from 2017 to 2019. The yellow shade represents the precipitation in wet season and the peak of pCO_2 in the cave and soil. (For interpretation of the references to colour in this figure legend, the reader is referred to the web version of this article.)

Table 2
Trace elements composition of cave water.

	Sample	Ca	Mg	Ba	Sr	Mg/Ca	Ba/Ca ($\times10^3$)	Sr/Ca ($\times10^3$)
Cave water	YZT (pool)	55.34	17.01	0.036	0.126	0.30	0.66	2.32
	YCG (pool)	63.02	30.39	0.031	0.088	0.50	0.53	1.47
	DTH (underground river)	49.92	14.85	0.033	0.118	0.29	0.66	2.36
	LYXS (drip)	99.30	32.66	0.019	0.084	0.34	0.19	0.85
	TGBD (drip)	83.62	34.78	0.022	0.092	0.45	0.22	0.95
	Mean	70.24	25.94	0.028	0.102	0.38	0.45	1.59
	Standard deviation	18.50	8.32	0.007	0.017	0.08	0.21	0.65

The elements units of cave water samples are $mg{\cdot}L^{-1}$.

The $\delta^{13}C$ values of the plant subsamples ranged from −23.3‰ to −28.1‰, with an average of −26.0 ± 1.1‰. The average $\delta^{13}C$ value of the organic matter in the soil subsamples collected from the soil profile was −16.7 ± 2.2‰, which is 9% higher than that of the plants.

4.6. DSY-1201 carbon isotope time series

The $\delta^{13}C$ records from stalagmite DSY-1201 in Dongshiya Cave cover the last ~200 years with an average resolution of ~1.5 months (Zhao et al., 2019). The $\delta^{13}C$ values range from −5.6‰ to −11.6‰ (average of −9.7‰). The large amplitude of the $\delta^{13}C$ record is consistent with the range of the modern calcite $\delta^{13}C$ values (−5.2‰ to −12.0‰) obtained from the monitoring and sample collection conducted between 2010 and 2019 for this study. Here, we only discuss the time period after 1950, i.e., 1950–2012.

5. Discussions

5.1. Factors affecting the cave water $\delta^{13}C_{DIC}$ on the seasonal scale

In general, the $\delta^{13}C_{DIC}$ values of cave water are effected by complex factors, including the CO_2 released by the respiration of vegetation roots, the decomposition of soil organic matter, bedrock carbonate dissolution, PCP and within-cave processes such as CO_2 degassing (Genty et al., 2001; Mickler et al., 2004; Spötl et al., 2005; Fairchild et al., 2006a; Frisia et al., 2011). All of these processes above are driven by the fractionation of the carbon isotopic, where CO_2 degassing from drip water causes the fractionation. The CO_2 degassing of the cave drip water depends on the cave air pCO_2, which is mainly controlled by the overlying soil CO_2 and cave ventilation (Spötl et al., 2005; Baldini et al., 2008; Lambert and Aharon, 2011; Pu et al., 2017). On the one hand, precipitation and consequently vegetation and soil activity (microbial activity and root respiration) are maximized during the wet season (Lechleitner et al., 2017), resulting in the highest relative humidity and soil pCO_2 during this period (Fig. 4). In principle, the enhanced

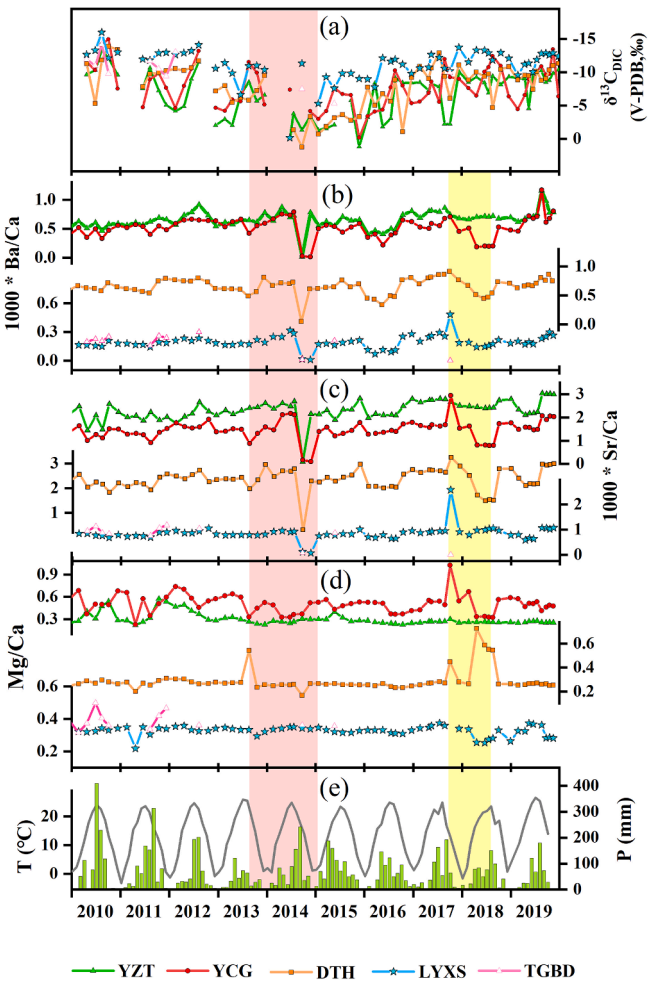

Fig. 5. The combined time series of meteoric conditions and the hydrogeochemistry of drip water. (a) the variation of cave water $\delta^{13}C_{DIC}$, (b) Ba/Ca ratios of cave water, (c) Sr/Ca ratios of cave water, (d) Mg/Ca ratios of cave water, (e) the monthly precipitation and the mean temperature outside the cave. The red and yellow column represent extreme drought events in 2013–2014 and 2017, respectively. (For interpretation of the references to colour in this figure legend, the reader is referred to the web version of this article.)

respiration of plant roots and the decomposition of microbes in the soil result in more ^{12}C CO_2 gas being dissolved in the soil water and eventually entering the cave (Li et al., 2012), which contributes to the negative values of $\delta^{13}C_{DIC}$. Conversely, the decrease of temperature and rainfall and biomass dormancy accounts for impoverishment of soil-derived CO_2 fluxes in winter (Fig. 4b). The amount of CO_2 dissolved in the groundwater decreases, resulting in a reduction of the air pCO_2 in Jiguan Cave (Fig. 4c), which leads to enhanced degassing of CO_2 from the solution and enriches drip water in ^{13}C. It seems that the variations in $\delta^{13}C_{DIC}$ values of cave water can be attribute to the variations of soil air CO_2 derived by local temperature and humid conditions.

However, the seasonal variations in the temperate and moist conditions are not completely synchronized with cave air CO_2 (Fig. 4a and c). This may be caused by the cave ventilation. In summer, the temperature of the cave air is lower than that of the external air, which causes a negative pressure gradient. The air stagnation in cave results in relatively weak ventilation effect and CO_2 build up in cave, thus increasing the cave air pCO_2 (Fig. 4c) and restricting the degassing of CO_2 from drip water (Spötl et al., 2005; Frisia et al., 2011; Dreybrodt et al., 2016). As a result, the drip water has more negative $\delta^{13}C$ values in summer, and vice versa in winter (Fig. 3a). Our results are consistent with the results of previous studies conducted in other caves such Obir Cave (Spötl et al., 2005), the Desoto Caverns (Lambert and Aharon, 2011), Furong Cave (Li et al., 2011), and Mawmluh Cave (Breitenbach et al., 2015). Actually, the timing and degree of degassing also affect the $\delta^{13}C$ values of cave water (Li et al., 2012). Given the longer degassing time of the pool water compared to that of the drip water, the $\delta^{13}C_{DIC}$ values of the pool water are more positive and the seasonal changes are more obvious than those of the drip water (Fig. 3). Therefore, we conclude that the seasonal variability of cave air pCO_2 caused by soil air CO_2 and cave ventilation are the major controlling factors for cave water $\delta^{13}C$ in Jiguan Cave.

5.2. *Factors affecting the $\delta^{13}C_{DIC}$ values and trace element compositions of the cave water on the annual scale*

The variation of cave water $\delta^{13}C_{DIC}$ responded to the changes of dry and wet conditions on interannual scales (Fig. 3). Generally, the precipitation infiltrates from the surface to a cave is usually accompanied by damping and the lag times of the preserved climate signal (Tooth and Fairchild, 2003; Fairchild et al., 2006b; Treble et al., 2013; Hu et al., 2020; Lyu et al., 2020a). As reported by Sun et al. (2018), the drips in Jiguan Cave mainly reflect the latest rainy precipitation in ordinary years, and the lag time from precipitation to drips is about 2 months (Liang et al., 2017). That means the residence time of seepage water from surface to cave is relative shorter, which may not affect the interannual signal of drip water $\delta^{13}C$. The wet years (2010 and 2015) experienced increased precipitation. In particular, in July and August 2010, the rainfall amounts successively reached the maximum monthly precipitation for that year (Fig. 3d). Large amounts of precipitation in a short period of time resulted in the groundwater move rapidly in the epikarst zone, which shortened the water–rock interaction time. The drip rate of cave water increased, PCP and CO_2 degassing were weakened, resulting in lower cave water $\delta^{13}C_{DIC}$ values (Fairchild et al., 2006a).

After 2010, the climate became dry, the precipitation decreased year by year, and the $\delta^{13}C_{DIC}$ values of cave water became increasingly positive (Fig. 3). In the extremely dry year (2013), the rainy precipitation was significantly less than usual and partly lost by evaporation in the soil. It is likely that cave water $\delta^{13}C$ values will reached to the heaviest as the severe drought. Actually, the most positive cave water $\delta^{13}C_{DIC}$ values and the highest trace element ratios appeared in 2014 (Fig. 5a), suggesting that a significant residence time of the water in the epikarst and the drips $\delta^{13}C$ reflect the combination of corresponding rainy precipitation and previous water in the overlying aquifer (Riechelmann et al., 2011). Our speculation is consistent with the results calculated by the bivariate model of oxygen isotope in Sun et al. (2018): The precipitation in 2013 was not directly converted into drip water and contributed to less than 10%. The contribution of 2014 to drips increased to ~40%, which corresponded to the rainfall recovery in the rainy season in 2014. Therefore, although before September 2014, the drip water in the cave was a mixture of "young precipitation water" provided by fracture flow and "old water", it still reflects the arid climate conditions. Given the decrease in precipitation caused by the drought during this period, the migration rate of atmospheric precipitation in the karst surface zone slowed down, the residence time of groundwater was prolonged, the water–rock interaction were strong, the time available for the cave water to dissolve the bedrock was long (Huang and Fairchild, 2001; Musgrove and Banner, 2004; Zhao et al., 2015). All of these factors combined together led to the higher $\delta^{13}C_{DIC}$ values of drip water.

The variability in trace elements ratios of drip water related to hydrological conditions is consistent with interannual drip water $\delta^{13}C_{DIC}$ variations (Fig. 5). Notably, significant peaks/valleys in trace element ratios usually occurred during the extreme dry-wet transition events, indicating that trace element ratios may be sensitive to hydrological changes from dry to wet conditions (Fig. 5). Because the drought lasted for more than a year (2013 ~ 2014), the pathway of groundwater may

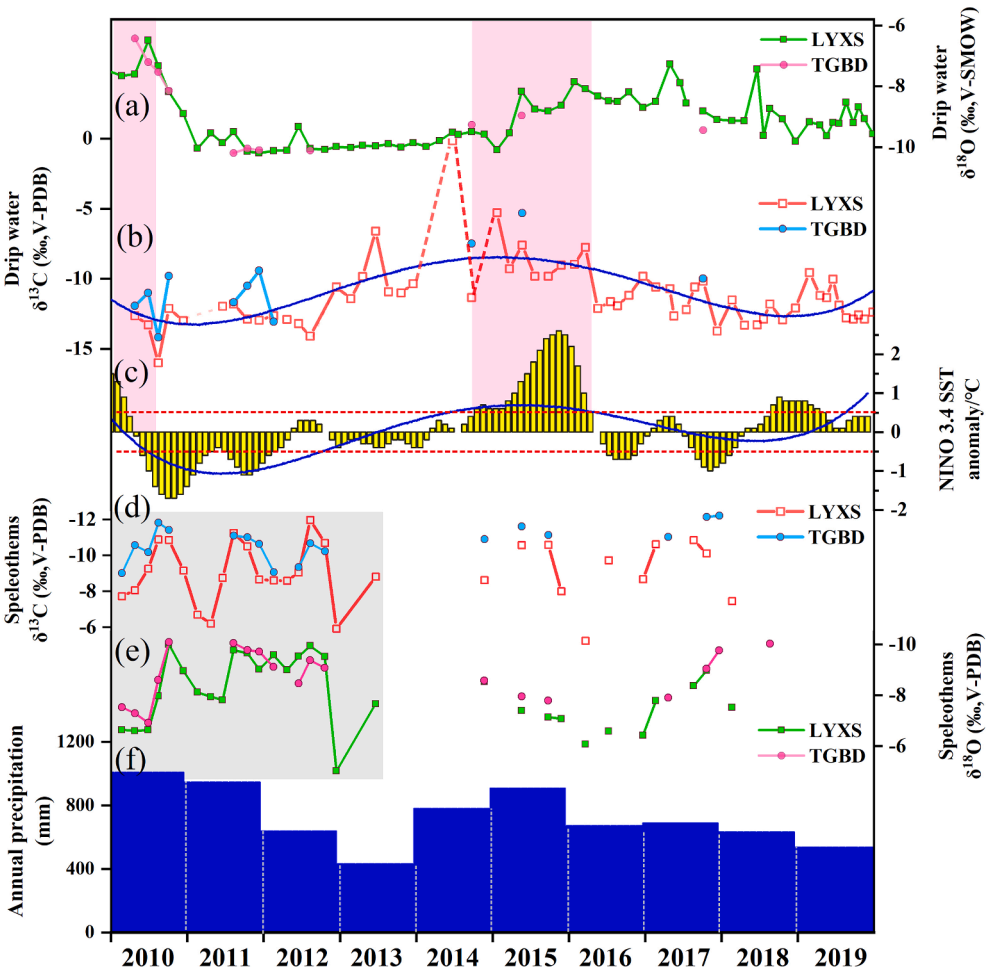

Fig. 6. Comparisons of drip water $\delta^{18}O$ (a), $\delta^{13}C_{DIC}$ (b), sea surface temperature anomaly (SSTA) of NINO 3.4 region from January 2010 to December 2019 (c), the modern speleothems $\delta^{13}C$ (d) and $\delta^{18}O$ (e) and annual precipitation (f). The blue curves in b and c are fourth order polynomial fitting results for drip water $\delta^{13}C_{DIC}$ and NINO 3.4 SSTA, respectively. The pink shades represent the changes of drip water $\delta^{18}O$ and $\delta^{13}C_{DIC}$ in two El Niño events. (For interpretation of the references to colour in this figure legend, the reader is referred to the web version of this article.)

have been relatively open in the epikarst zone, which facilitated the degassing of CO_2 and the deposition of carbonate along the flow path (Wong et al., 2011). As the water–rock interaction increased, more bedrock was dissolved and more Mg^{2+} was released into the groundwater (Fairchild et al., 2000). Moreover, the preferential deposition of Ca^{2+} over Mg^{2+} and Sr^{2+} caused by PCP resulted in higher Mg/Ca ratios (Karmann et al., 2007; Wong et al., 2011; Tremaine and Froelich, 2013; Casteel and Banner, 2015). In contrast, the precipitation increased after the long period of drought (Fig. 5e), the groundwater penetrated the soil and bedrock more rapidly, shortening the water–rock interaction time. The increased rate of bedrock dissolution caused the higher metal ions concentrations in drip water, leading to a decrease of the Ba /Ca, Sr/Ca and Mg/Ca (Fig. 5b, c and d).

The cave air pCO_2 is also an important factor affecting the trace element ratios of cave water (Banner et al., 2007; Sherwin and Baldini, 2011; Wong et al., 2011; Treble et al., 2015). The monitoring results revealed that the average cave air pCO_2 values exhibited obvious variations, which were consistent with the temperature and precipitation variations. In particular, in 2019 (a drought year), there was a sharp decrease (Fig. 4c). On the one hand, the variations in the cave air pCO_2 were mainly affected by the natural environment outside the cave and were controlled by the changes in the CO_2 content of the overlying soil, whereas the soil CO_2 concentration was affected by the root respiration and the biological activity in the overlying soil (Knorr et al., 2005; Davidson et al., 2006). On the other hand, the changes of cave air pCO_2 may be caused by cave ventilation (Spötl et al., 2005; Lyu et al., 2020b). However, the ventilation type of stagnant in summer and flowing in winter in Jiguan Cave had little influence on the interannual variation of cave air pCO_2. Therefore, temperature and precipitation may be significant factors affecting the air pCO_2 in Jiguan Cave on interannual scales. After the extreme drought, biological activity increased as the recovery of precipitation recovered starting in June 2014, resulting in a large amount of soil CO_2 entering the cave through the groundwater and cracks, increasing the CO_2 content of the cave air, which inhibited CO_2 degassing from the cave water (Baldini et al., 2008), and finally caused a decrease in the Sr/Ca, Ba/Ca, and Mg/Ca ratios (Fig. 5). Therefore, we suspect that the variations in the $\delta^{13}C_{DIC}$ values and trace element ratios of the cave water were consistent with the changes in the local hydrological conditions.

5.3. *The response of carbon isotope composition of the drip water to ENSO*

The 10-year monitoring period experienced two complete ENSO cycles from El Niño in 2010 to La Niña in 2011, and from strong El Niño in 2015 to La Niña in 2017 and a weaker El Niño that resumed in 2018. The $\delta^{13}C_{DIC}$ values of the drip water were quite consistent with the ENSO (Fig. 6b and c). The average $\delta^{13}C_{DIC}$ values of drip water were continuously enriched from the most negative value in 2010 (-12.7‰) to −4.8‰ in 2014. Then, they gradually became more negative after 2014 and enriched again after 2018 (Table 3). Moreover, the $\delta^{13}C_{DIC}$ values of two drip water sites correlated well with the NINO 3.4 SST anomaly (Table 4), indicating that the cave drip water $\delta^{13}C_{DIC}$ may respond to the transformation of ENSO.

The interannual variations of precipitation $\delta^{18}O$ values at Jiguan Cave were influenced by ENSO, which is derived by circulation effect (Sun et al., 2018). Sun et al. (2018) suggested that El Niño years are more influenced by moisture from the proximal source (i.e., the west

Table 3
Mean $\delta^{13}C_{DIC}$ of drip water (V-PDB/‰).

	2010	2011	2012	2013	2014	2015	2016	2017	2018	2019
Jan						−5.3	−9.0			
Feb			−12.6	−11.4				−10.6	−11.5	−9.6
Mar						−9.3	−7.8			
Apr	−12.3		−12.9	−9.9				−10.7	−13.3	−11.2
May						−6.5	−12.1	−12.7		−11.4
Jun	−12.1	−12.0	−13.2	−6.6	−0.2				−13.3	−10.0
July						−9.9	−11.6	−12.2	−12.9	−11.9
Aug	−15.1	−11.7	−14.1	−11.0			−11.9	−10.6	−11.8	−12.8
Sep					−9.4	−9.9				−12.9
Oct	−11.0	−11.7		−11.0			−11.2	−10.1	−12.9	−12.6
Nov						−9.0				−12.9
Dec	−13.0	−11.2	−10.6	−10.4			−9.8	−13.7	−12.1	−12.4
annual	−12.7	−11.7	−12.7	−10.0	−4.8	−8.3	−10.5	−11.5	−12.5	−11.8

Table 4
Correlation coefficients between SSTA, LYXS $\delta^{13}C_{DIC}$ and TGBD $\delta^{13}C_{DIC}$ from 2010 to 2019.

r	SSTA	LYXS	TGBD
SSTA	1	0.360**	0.620*
LYXS		1	0.822**
TGBD			1

The sample number of SSTA, LYXS and TGBD is 121, 60 and 12, respectively.
* Indicates significant at a 95% confidence level ($p < 0.05$).
** Indicates significant at a 99% confidence level ($p < 0.01$).

Pacific), whereas La Niña years are more affected by moisture from the remote source (i.e., the Indian Ocean). Although there was no seasonal variation in drip water $\delta^{18}O$, it exhibited dramatic changes in 2010 and 2015 (Fig. 6a). Interestingly, the variation in the $\delta^{13}C_{DIC}$ values of the drip water was opposite to the variation in the $\delta^{18}O$ values during these two periods. A rapid increase was observed after June 2010, and a rapid decrease was observed in 2015 (Fig. 6b).

Previous studies have suggested that there may be more precipitation in eastern Asia during El Niño decay years (Ju and Slingo, 1995; Zheng and Zhu, 2015). The year 2010 was an El Niño decay year, and the El Niño event in 2015 was the most powerful in this century, the precipitation increased significantly (Fig. 6f). Owing to the higher precipitation, the microbial activity in the soil was stronger, the soil CO_2 production rate was higher (Li and Li, 2018), the atmospheric precipitation dissolved more soil CO_2 that contains partial negative ^{13}C into the epikarst zone, and the $\delta^{13}C_{DIC}$ value of drip water was significantly lower (Fig. 6b). Therefore, the rainfall amount is responsible for the $\delta^{13}C_{DIC}$ of the drip water. In summary, the $\delta^{13}C_{DIC}$ and $\delta^{18}O$ values exhibit opposite trends, but both indirectly respond to the large-scale atmospheric circulation conditions.

5.4. *Transportation of carbon isotope signals within the karst cave system*

In general, all of the $\delta^{13}C$ values of the plants (−28.1‰ to −23.3‰) above Jiguan Cave fall within the range of modern C3 vegetation (i.e., −20‰ to −35‰) (Deines, 1980; Cerling, 1984; Staddon, 2004). Therefore, the plants overlying Jiguan Cave are typical C3 plants characterized by distinct negative $\delta^{13}C$ values. The isotope fractionation that occurs during the decomposition of soil organic matter by microbes results in an unequal distribution of ^{13}C and ^{12}C carbon isotopes in the different carbon phases (Trumbore, 2000). Relatively more light isotopes (^{12}C) would transform into the released CO_2, and more ^{13}C enters the organic matter of microbes and eventually returns to the soil organic matter (Luo and Wang, 2009; Li et al., 2012). The wet and hot season promotes the decomposition of microorganisms in the soil, resulting in higher $\delta^{13}C$ of soil organic matter than the overlying plants (Fig. 7). The enrichment from the soil layer to the drip water (approximately 5‰) indicates a sufficient isotopic exchange between the DIC in soil water

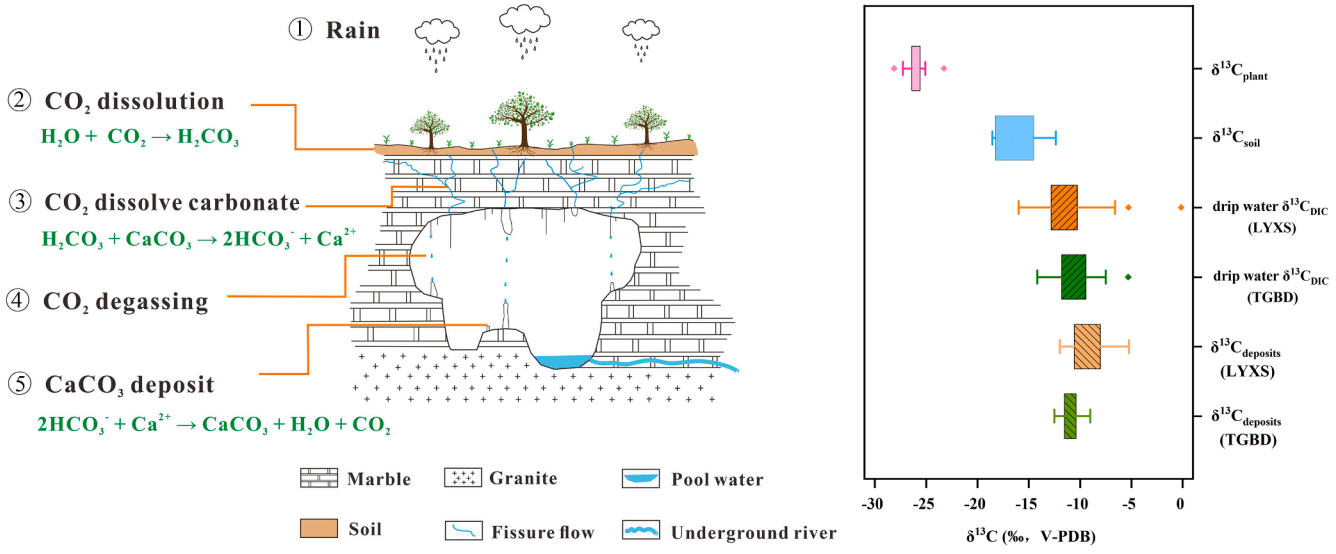

Fig. 7. Schematic of the transport mechanism of $\delta^{13}C$ in the Jiguan Cave system, from the plants to soil to drip water and to modern deposits. Variation of $\delta^{13}C$ transport in the cave system. The upper and lower points of each box pattern represent the maximum and minimum values of the group of data, the diamonds represent outliers.

and the CO_2 in soil (Baker et al., 1997; Fairchild et al., 2006a). The process of soil water migrating through the fracture pipes to form cave drip water is influenced by water–rock interaction and PCP (Tooth and Fairchild, 2003). Karst water dissolved more bedrock with heavier ^{13}C during the migration of the epikarst zone because of CO_2 degassing from seepage water and the promotion of calcite precipitation, resulting in more positive $\delta^{13}C_{DIC}$ values of the drip water.

When the drip water dripped, due to the lower pCO_2 within cave and supersaturated drip water to calcite, CO_2 escaped from drip water, resulting in the precipitation of speleothems ($CaCO_3$) (Hendy, 1971; Luo and Wang, 2009). Thus the $\delta^{13}C$ values of the modern speleothem are more positive than drip water (Fig. 7). A previous study in Jiguan Cave suggested that the speleothems inherited the signal of drip water, and the ENSO-driven precipitation $\delta^{18}O$ variations can be transferred to modern speleothems by drips (Sun et al., 2018). According to the analysis in Section 5.3, $\delta^{13}C$ and $\delta^{18}O$ values of drip water can response to ENSO. The synchronous changes in the $\delta^{13}C$ and $\delta^{18}O$ values of the modern speleothems, especially significant decreases in the $\delta^{13}C$ and $\delta^{18}O$ values in 2013 (extremely drought year) (Fig. 6d and e), indicating that the $\delta^{13}C$ signal of speleothem also is affected by temperature and precipitation which may be related to ENSO.

5.5. Implications for paleoclimate reconstruction from stalagmite record

The processes and factors governing the $\delta^{13}C_{DIC}$ variability of cave water have important implications for the interpretation of $\delta^{13}C$ time-series in speleothems as proxy records of climate driven carbon transport changes in cave environments (Lambert and Aharon, 2011). Speleothem $\delta^{13}C$ values have a large biogenic component originating from vegetation and soil activity above the cave, which are strongly dependent on the amount of precipitation and local air temperature (Fohlmeister et al., 2020). Although the $\delta^{13}C$ signal may be disturbed by many inorganic factors, these factors are also mainly driven by the changes of local climate and environment (McDermott, 2004; Fairchild et al., 2006a; Li et al., 2018, 2020; Tan et al., 2020a, 2020b).

The $\delta^{13}C$ record of stalagmite DSY-1201 and the precipitation record for this area show obvious synchronous changes over the past 60 years, with lower $\delta^{13}C$ values in wet years and higher values in drought years (Fig. 8). The changes of vegetation types above the cave can be ruled out as the primary cause of the variation in stalagmite $\delta^{13}C$ since these

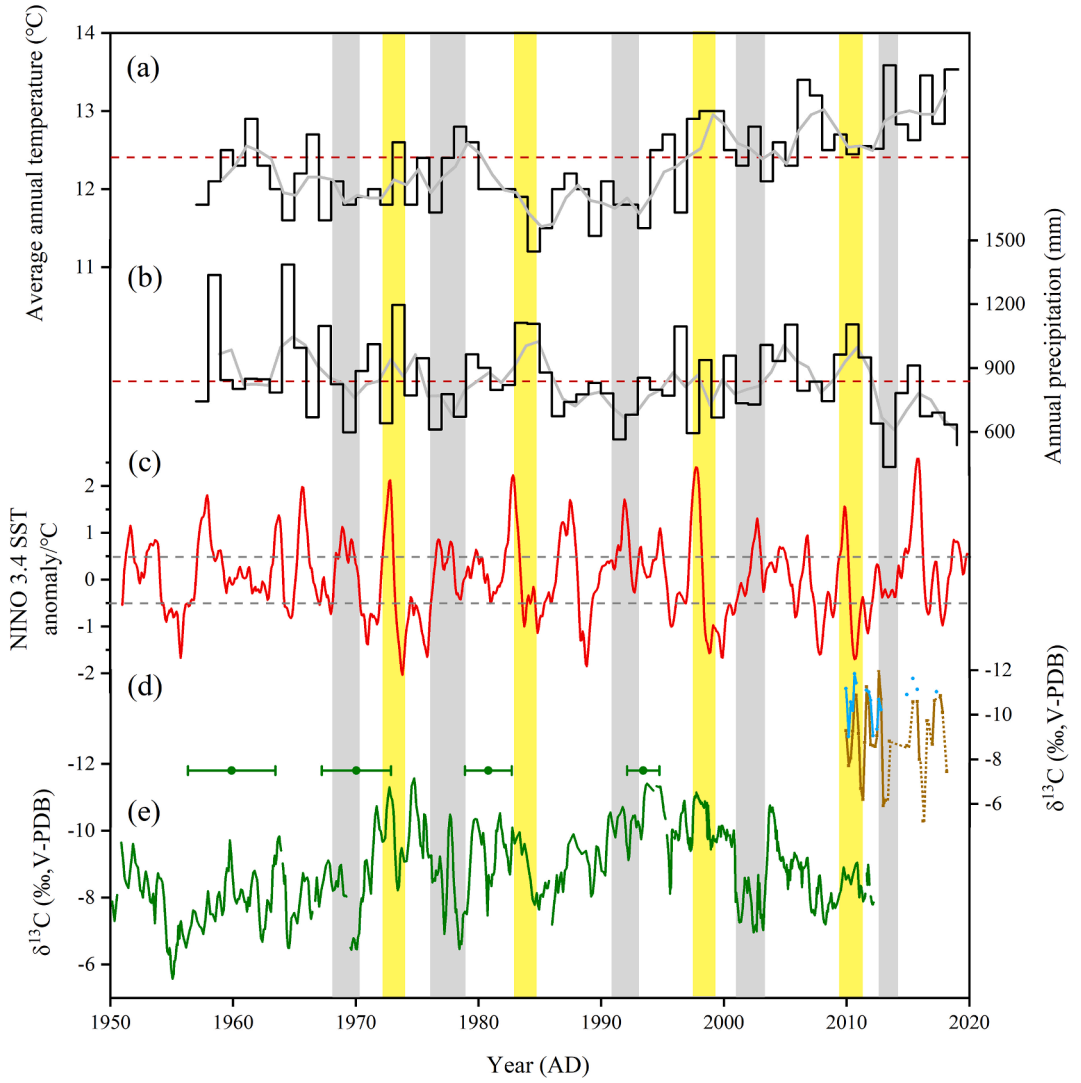

Fig. 8. The mean annual temperature (a) and annual precipitation (b) in Luanchuan from 1957 to 2019. The red dotted line and the gray line represent the mean value of 63-year and the 3-point running means, respectively. (c) Sea surface temperature (SST) anomaly of NINO 3.4 region. (d) The modern speleothems $\delta^{13}C$ from Jiguan Cave, the brown and blue line represent LYXS and TGBD, respectively. The brown dotted line represents the trend of missing data in LYXS. (e) The $\delta^{13}C$ records from stalagmite DSY-1201, the green error bar represents the age error of stalagmite. The yellow and grey shades represent ENSO events and drought years, respectively. (For interpretation of the references to colour in this figure legend, the reader is referred to the web version of this article.)

changes would occur on a longer time scale rather than on decadal-scale. Vegetation density and karst processes are more suitable explanations for the observed variations in DSY-1201 $\delta^{13}C$ values. During the dry period, lower levels of precipitation reduced vegetation cover and density, and the higher temperature enhanced evaporation, which can quickly reduce the water stored in soils and decrease the plant root respiration and soil organic matter content (Cosford et al., 2009; Kennett et al., 2012; Lechleitner et al., 2017; Fohlmeister et al., 2020), resulting in more positive $\delta^{13}C$ values in drip water and speleothems. Moreover, a dry climate would increase residence time of the seepage water and favor more bedrock dissolution (McDermott, 2004; Rudzka et al., 2011; Tan et al., 2013). In addition, enhanced PCP in the vadose zone above the cave prolongs the CO_2 degassing within the cave (Bar-Matthews et al., 1996; Baker et al., 1997; Tan et al., 2020a), all these factors taken together result in the positive $\delta^{13}C$ values. On the contrary, wet climate conditions benefit vegetation growth and biological productivity, resulting in higher soil activity (more input of isotopically light organic carbon into soil water) and weaker the water-rack interaction and CO_2 degassing, which may contribute to the relatively low $\delta^{13}C$ values (Genty et al., 2003; McDermott, 2004). Therefore, stalagmite $\delta^{13}C$ are tightly connected to local climate conditions.

There may be more precipitation in eastern Asia during El Niño decay years (Ju and Slingo, 1995; Zheng and Zhu, 2015). Thus, the wet years correspond to ENSO conversion years, i.e. the transition of El Niño events to La Niña events (Fig. 8a and c). Our observations argue in favor of that a climate-driven shift in hydrogeochemical effects as the dominant factor governing the long-term changes of speleothem $\delta^{13}C$ on the decadal scale. Therefore, we suggest that stalagmite $\delta^{13}C$ can be a potential proxy that reflects the changes of precipitation and indirectly responds to the transformation of ENSO.

6. Conclusions

Based on the continuous monitoring of Jiguan Cave from 2010 to 2019, we reached the following conclusions:

(1) The $\delta^{13}C_{DIC}$ values of cave water exhibited both the seasonal and interannual variations. The relatively high humidity and soil pCO_2 and air stagnation in cave caused more negative $\delta^{13}C$ values of cave water during summer and vice versa in winter. The carbon isotopes and trace element ratios of the cave water reflect the wet/dry conditions and are sensitive to extreme drought events caused by the decrease in summer monsoon precipitation on the interannual scales.

(2) The carbon isotope compositions in karst cave systems are continuously enriched when migrating from the vegetation to the soil to the cave drip water to the modern deposits. Although both $\delta^{13}C$ and $\delta^{18}O$ of the drip water respond to ENSO, the $\delta^{13}C$ is mainly affected by local precipitation induced by ENSO, while the $\delta^{18}O$ drip water can record the variation of precipitation $\delta^{18}O$ by 'circulation effect'. The ENSO indirectly drives the interannual pattern of drip water $\delta^{13}C$, which can be transferred to speleothems.

(3) Precipitation is the dominant factor controlling the residence time of the seepage water, future affect the bedrock dissolution, PCP in the unsaturated zone above the cave and the degassing of CO_2 within the cave, which finally influenced the $\delta^{13}C$ values of stalagmite DSY-1201 on the decadal scale. Carbon isotopes in stalagmite can be a potential proxy related to local hydrological climate and indirectly reflect ENSO.

CRediT authorship contribution statement

Yidong Li: Writing - original draft, Formal analysis, Investigation. **Yan Yang:** Formal analysis, Investigation, Writing - review & editing. **Xiuyang Jiang:** Investigation, Writing - review & editing. **Jingyao Zhao:** Investigation, Writing - review & editing. **Zhe Sun:** Investigation, Writing - review & editing. **Xiao Shi:** Investigation. **Ning Tian:** Investigation. **Yunyue Yang:** Investigation. **Jiancang Li:** Resources. **Junwei Duan:** Resources.

Declaration of Competing Interest

The authors declare that they have no known competing financial interests or personal relationships that could have appeared to influence the work reported in this paper.

Acknowledgements

This work was supported by grants of the National Natural Science Foundation of China (Nos 41877450, 41672160, 41372177, 40902053). We thank to the staff of Jiguan Cave Tourism Development Limited in Luanchuan County, Henan Province, for their supports in sampling.

Appendix A. Supplementary data

Supplementary data to this article can be found online at https://doi.org/10.1016/j.jhydrol.2020.125841.

References

Baker, A., Brunsdon, C., 2003. Non-linearities in drip water hydrology: an example from Stump Cross Caverns, Yorkshire. J. Hydrol. 277, 151–163.
Baker, A., Ito, E., Smart, P.L., McEwan, R.F., 1997. Elevated and variable values of ^{13}C in speleothems in a British cave system. Chem. Geol. 136, 263–270.
Baldini, J.U.L., Mcdermott, F., Hoffmann, D.L., Richards, D.A., Clipson, N., 2008. Very high-frequency and seasonal cave atmosphere PCO_2 variability: Implications for stalagmite growth and oxygen isotope-based paleoclimate records. Earth Planetary Sci. Lett. 272, 118–129.
Banner, J.L., Guilfoyle, A., James, E.W., Stern, L.A., Musgrove, M., 2007. Seasonal variations in modern speleothem calcite growth in Central Texas, USA. J. Sediment. Res. 77, 615–622.
Bar-Matthews, M., Ayalon, A., Kaufman, A., 1997. Late Quaternary Paleoclimate in the Eastern Mediterranean Region from Stable Isotope Analysis of Speleothems at Soreq Cave, Israel. Quat. Res. 47, 155–168.
Bar-Matthews, M., Ayalon, A., Kaufman, A., Wasserburg, G.J., 1999. The Eastern Mediterranean paleoclimate as a reflection of regional events: Soreq cave, Israel. Earth Planet. Sci. Lett. 166, 85–95.
Bar-Matthews, M., Ayalon, A., Matthews, A., Sass, E., Halicz, L., 1996. Carbon and oxygen isotope study of the active water-carbonate system in a karstic Mediterranean cave: Implications for paleoclimate research in semiarid regions. Geochim. Cosmochim. Acta 60, 337–347.
Breitenbach, S.F.M., Lechleitner, F.A., Meyer, H., Diengdoh, G., Mattey, D., Marwan, N., 2015. Cave ventilation and rainfall signals in dripwater in a monsoonal setting – a monitoring study from NE India. Chem. Geol. 402, 111–124.
Cai, Y.J., Tan, L.C., Cheng, H., An, Z.S., Edwards, R.L., Kelly, M.J., Kong, X.G., Wang, X. F., 2010. The variation of summer monsoon precipitation in central China since the last deglaciation. Earth Planet. Sci. Lett. 291, 21–31.
Casteel, R.C., Banner, J.L., 2015. Temperature-driven seasonal calcite growth and drip water trace element variations in a well-ventilated Texas cave: Implications for speleothem paleoclimate studies. Chem. Geol. 392, 43–58.
Cerling, T.E., 1984. The stable isotopic composition of modern soil carbonate and its relationship to climate. Earth Planet. Sci. Lett. 71, 229–240.
Chen, C.J., Li, T.Y., 2018. Geochemical characteristics of cave drip water respond to ENSO based on a 6-year monitoring work in Yangkou Cave, Southwest China. J. Hydrol. 561, 896–907.
Cheng, H., Edwards, R.L., Broecker, W.S., Denton, G.H., Kong, X., Wang, Y., Zhang, R., Wang, X., 2009. Ice age terminations. Science 326, 248–252.
Cheng, H., Edwards, R.L., Sinha, A., Spötl, C., Yi, L., Chen, S., Kelly, M., Kathayat, G., Wang, X., Li, X., Kong, X., Wang, Y., Ning, Y., Zhang, H., 2016. The Asian monsoon over the past 640,000 years and ice age terminations. Nature 534, 640–646.
Cobb, K.M., Adkins, J.F., Partin, J.W., Clark, B., 2007. Regional-scale climate influences on temporal variations of rainwater and cave dripwater oxygen isotopes in northern Borneo. Earth Planet. Sci. Lett. 263, 207–220.
Coplen, T.B., Winograd, I.J., Landwehr, J.M., Riggs, A.C., 1994. 500,000-Year stable carbon isotopic record from Devils-Hole, Nevada. Science 263, 361–365.
Cosford, J., Qing, H.R., Mattey, D., Eglington, B., Zhang, M.L., 2009. Climatic and local effects on stalagmite $\delta^{13}C$ values at Lianhua Cave, China. Palaeogeogr. Palaeoclimatol. Palaeoecol. 280, 235–244.
Davidson, E.A., Janssens, I.A., Luo, Y., 2006. On the variability of respiration in terrestrial ecosystems: moving beyond Q10. Glob. Change Biol. 12, 154–164.
Deines, P., 1980. Chapter 9 – The isotopic composition of reduced organic carbon. In: Fritz, P., Fontes, J.C. (Eds.), The Terrestrial Environment. A. Elsevier, Amsterdam, pp. 329–406.

Dorale, J., Gonzalez, L., Reagan, M., Pickett, D., Murrell, M., Baker, R., 1992. A high-resolution record of holocene climate change in speleothem calcite from Cold Water Cave, Northeast Iowa. Science 258, 1626–1630.
Dorale, J.A., Edwards, R.L., Ito, E., González, L.A., 1998. Climate and vegetation history of the midcontinent from 75 to 25 ka: a speleothem record from crevice cave, Missouri, USA. Science 282, 1871–1874.
Dreybrodt, W., Hansen, M., Scholz, D., 2016. Processes affecting the stable isotope composition of calcite during precipitation on the surface of stalagmites: laboratory experiments investigating the isotope exchange between DIC in the solution layer on top of a speleothem and the CO_2 of the cave atmosphere. Geochim. Cosmochim. Acta 174, 247–262.
Fairchild, I.J., Borsato, A., Tooth, A.F., Frisia, S., Hawkesworth, C.J., Huang, Y.M., McDermott, F., Spiro, B., 2000. Controls on trace element (Sr-Mg) compositions of carbonate cave waters: implications for speleothem climatic records. Chem. Geol. 166, 255–269.
Fairchild, I.J., Smith, C.L., Baker, A., Fuller, L., Spötl, C., Mattey, D., McDermott, F., E.I. M.F, 2006a. Modification and preservation of environmental signals in speleothems. Earth-Sci. Rev. 75, 105–153.
Fairchild, I.J., Treble, P.C., 2009. Trace elements in speleothems as recorders of environmental change. Quat. Sci. Rev. 28, 449–468.
Fairchild, I.J., Tuckwell, G.W., Baker, A., Tooth, A.F., 2006b. Modelling of dripwater hydrology and hydrogeochemistry in a weakly karstified aquifer (Bath, UK): implications for climate change studies. J. Hydrol. 321, 213–231.
Feng, W.M., Casteel, R.C., Banner, J.L., Heinze-Fry, A., 2014. Oxygen isotope variations in rainfall, drip-water and speleothem calcite from a well-ventilated cave in Texas, USA: assessing a new speleothem temperature proxy. Geochim. Cosmochim. Acta 127, 233–250.
Fleitmann, D., Cheng, H., Badertscher, S., Edwards, R.L., Mudelsee, M., Goektuerk, O.M., Fankhauser, A., Pickering, R., Raible, C.C., Matter, A., Kramers, J., Tuysuz, O., 2009. Timing and climatic impact of Greenland interstadials recorded in stalagmites from northern Turkey. Geophys. Res. Lett. 36, L19707.
Fohlmeister, J., Plessen, B., Dudashvili, A.S., Tjallingii, R., Wolff, C., Gafurov, A., Cheng, H., 2017. Winter precipitation changes during the Medieval Climate Anomaly and the Little Ice Age in arid Central Asia. Quat. Sci. Rev. 178, 24–36.
Fohlmeister, J., Voarintsoa, N.R.G., Lechleitner, F.A., Boyd, M., Brandtstätter, S., Jacobson, M.J., Oster, J.L., 2020. Main controls on the stable carbon isotope composition of speleothems. Geochim. Cosmochim. Acta 279, 67–87.
Frappier, A.B., 2013. Masking of interannual climate proxy signals by residual tropical cyclone rainwater: Evidence and challenges for low-latitude speleothem paleoclimatology. Geochem. Geophys. Geosyst. 14, 3632–3647.
Frisia, S., Fairchild, I.J., Fohlmeister, J., Miorandi, R., Spötl, C., Borsato, A., 2011. Carbon mass-balance modelling and carbon isotope exchange processes in dynamic caves. Geochim. Cosmochim. Acta 75, 380–400.
Fuller, L., Baker, A., Fairchild, I.J., Spötl, C., Marca-Bell, A., Rowe, P., Dennis, P.F., 2008. Isotope hydrology of dripwaters in a Scottish cave and implications for stalagmite palaeoclimate research. Hydrol. Earth Syst. Sci. Discuss. 5, 547–577.
Genty, D., Baker, A., Massault, M., Proctor, C., Gilmour, M., Pons-Branchu, E., Hamelin, B., 2001. Dead carbon in stalagmites: carbonate bedrock paleodissolution vs. ageing of soil organic matter. Implications for ^{13}C variations in speleothems. Geochim. Cosmochim. Acta 65, 3443–3457.
Genty, D., Blamart, D., Ouahdi, R., Gilmour, M., Baker, A., Jouzel, J., Van-Exter, S., 2003. Precise dating of Dansgaard-Oeschger climate oscillations in western Europe from stalagmite data. Nature 421, 833–837.
Genty, D., Massault, M., 1999. Carbon transfer dynamics from bomb-^{14}C and $\delta^{13}C$ time series of a laminated stalagmite from SW France—modelling and comparison with other stalagmite records. Geochim. Cosmochim. Acta 63, 1537–1548.
Goldsmith, Y., Broecker, W.S., Xu, H., Polissar, P.J., Demenocal, P.B., Porat, N., Lan, J., Cheng, P., Zhou, W., An, Z., 2017. Northward extent of East Asian monsoon covaries with intensity on orbital and millennial timescales. Proc. Natl. Acad. Sci. 114, 1817–1821.
Hellstrom, J.C., McCulloch, M.T., 2000. Multi-proxy constraints on the climatic significance of trace element records from a New Zealand speleothem. Earth Planet. Sci. Lett. 179, 287–297.
Hendy, C.H., 1971. The isotopic geochemistry of speleothems—I. The calculation of the effects of different modes of formation on the isotopic composition of speleothems and their applicability as palaeoclimatic indicators. Geochim. Cosmochim. Acta 35, 801–824.
Hu, C., Henderson, G.M., Huang, J., Xie, S., Sun, Y., Johnson, K.R., 2008. Quantification of Holocene Asian monsoon rainfall from spatially separated cave records. Earth Planet. Sci. Lett. 266, 221–232.
Hu, Y.D., Liu, Z.H., Ford, D., Zhao, M., Bao, Q., Zeng, C., Gong, X.Y., Wei, Y., Cai, X.L., Chen, J., 2020. Conservation of oxygen and hydrogen seasonal isotopic signals in meteoric precipitation in groundwater: An experimental tank study of the effects of land cover in a summer monsoon climate. Geochim. Cosmochim. Acta 284, 254–272.
Huang, Y.M., Fairchild, I.J., 2001. Partitioning of Sr^{2+} and Mg^{2+} into calcite under karst-analogue experimental conditions. Geochim. Cosmochim. Acta 65, 47–62.
Ju, J.H., Slingo, J., 1995. The Asian summer monsoon and ENSO. Q. J. R. Meteorolog. Soc. 121, 1133–1168.
Karmann, I., Cruz, F.W., Viana, O., Burns, S.J., 2007. Climate influence on geochemistry parameters of waters from Santana-Pérolas cave system, Brazil. Chem. Geol. 244, 232–247.
Kennett, D.J., Breitenbach, S.F.M., Aquino, V.V., Asmerom, Y., Awe, J., Baldini, J.U.L., Bartlein, P., Culleton, B.J., Ebert, C., Jazwa, C., Macri, M.J., Marwan, N., Polyak, V., Prufer, K.M., Ridley, H.E., Sodemann, H., Winterhalder, B., Haug, G.H., 2012. Development and disintegration of Maya political systems in response to climate change. Science 338, 788–791.
Knorr, W., Prentice, I.C., House, J.I., Holland, E.A., 2005. Long-term sensitivity of soil carbon turnover to warming. Nature 433, 298–301.
Lambert, W.J., Aharon, P., 2011. Controls on dissolved inorganic carbon and $\delta^{13}C$ in cave waters from DeSoto Caverns: Implications for speleothem $\delta^{13}C$ assessments. Geochim. Cosmochim. Acta 75, 753–768.
Lechleitner, F.A., Breitenbach, S.F.M., Cheng, H., Plessen, B., Rehfeld, K., Goswami, B., Marwan, N., Eroglu, D., Adkins, J., Haug, G., 2017. Climatic and in-cave influences on $\delta^{18}O$ and $\delta^{13}C$ in a stalagmite from northeastern India through the last deglaciation. Quat. Res. 88, 458–471.
Li, J.Y., Li, T.Y., 2018. Seasonal and annual changes in soil/cave air pCO_2 and the $\delta^{13}C_{DIC}$ of cave drip water in response to changes in temperature and rainfall. Appl. Geochem. 93, 94–101.
Li, T.Y., Huang, C.X., Tian, L.J., Suarez, M., Gao, Y.L., 2018. Variation of $\delta^{13}C$ in plant-soil-cave systems in karst regions with different degrees of rocky desertification in southwest China. J. Cave Karst Stud. 80, 212–228.
Li, T.Y., Li, H.C., Xiang, X.J., Kuo, T.S., Li, J.Y., Zhou, F.L., Chen, H.L., Peng, L.L., 2012. Transportation characteristics of $\delta^{13}C$ in the plants-soil-bedrock-cave system in Chongqing karst area. Sci. China Earth Sci. 55, 685–694.
Li, T.Y., Shen, C.C., Li, H.C., Li, J.Y., Chiang, H.W., Song, S.R., Yuan, D.X., Lin, C.D.J., Gao, P., Zhou, L., Wang, J.L., Ye, M.Y., Tang, L.L., Xie, S.Y., 2011. Oxygen and carbon isotopic systematics of aragonite speleothems and water in Furong Cave, Chongqing, China. Geochim. Cosmochim. Acta 75, 4140–4156.
Li, Y.X., Rao, Z.G., Xu, Q.H., Zhang, S.R., Liu, X.K., Wang, Z.L., Cheng, H., Edwards, R.L., Chen, F.H., 2020. Inter-relationship and environmental significance of stalagmite $\delta^{13}C$ and $\delta^{18}O$ records from Zhenzhu Cave, north China, over the last 130 ka. Earth Planet. Sci. Lett. 536, 116149.
Liang, S., Yang, Y., Zhang, N., Sun, Z., Zhang, P., Tian, N., Ling, X.Y., Ren, X.M., 2017. Analysis of temporal and spatial variations in trace element migration in karst critical zone: an example of Jiguan Cave, Henan. Environ. Sci. 38 (10), 4130–4140 (in Chinese with English abstract).
Liu, D.B., Wang, Y.J., Cheng, H., Edwards, R.L., Kong, X.G., Li, T.Y., 2016. Strong coupling of centennial-scale changes of Asian monsoon and soil processes derived from stalagmite $\delta^{18}O$ and $\delta^{13}C$ records, southern China. Quat. Res. 85, 333–346.
Liu, X.K., Liu, J.B., Chen, S.Q., Chen, J.H., Zhang, X., Yan, J.J., Chen, F.H., 2020. New insights on Chinese cave $\delta^{18}O$ records and their paleoclimatic significance. Earth Sci. Rev. 207, 103216.
Luo, W.J., Wang, S.J., 2009. Transmission of $\delta^{13}C$ signals and its paleoclimatic implications in Liangfeng Cave system of Guizhou Province, SW China. Environ. Earth Sci. 59, 655–661.
Lyu, Y.N., Luo, W.J., Wang, Y.W., Zeng, G.N., Cai, X.L., Wang, M.F., Chen, J., Yang, K.P., Weng, X., Cheng, A.Y., Zhang, L., Zhang, R.Y., Wang, S.J., 2020a. Geochemical responses of cave drip water to vegetation restoration. J. Hydrol. 590, 125543.
Lyu, Y.N., Luo, W.J., Wang, Y.W., Zeng, G.N., Wang, Y., Cheng, A.Y., Zhang, L., Chen, J., Cai, X.L., Zhang, R.Y., Wang, S.J., 2020b. Impacts of cave ventilation on drip water $\delta^{13}C_{DIC}$ and its paleoclimate implication. Quat. Int. 547, 7–21.
Maher, B.A., 2008. Holocene variability of the East Asian summer monsoon from Chinese cave records: a re-assessment. Holocene 18, 861–866.
Maher, B.A., Thompson, R., 2012. Oxygen isotopes from Chinese caves: records not of monsoon rainfall but of circulation regime. J Quat Sci. J. Quat. Sci. 27, 615–624.
McDermott, F., 2004. Palaeo-climate reconstruction from stable isotope variations in speleothems: a review. Quat. Sci. Rev. 23, 901–918.
Mickler, P.J., Banner, J.L., Stern, L., Asmerom, Y., Edwards, R.L., Ito, E., 2004. Stable isotope variations in modern tropical speleothems: Evaluating equilibrium vs. kinetic isotope effects. Geochim. Cosmochim. Acta 68, 4381–4393.
Musgrove, M., Banner, J.L., 2004. Controls on the spatial and temporal variability of vadose dripwater geochemistry: Edwards aquifer, central Texas. Geochim. Cosmochim. Acta 68, 1007–1020.
Oster, J.L., Montañez, I.P., Guilderson, T.P., Sharp, W.D., Banner, J.L., 2010. Modeling speleothem $\delta^{13}C$ variability in a central Sierra Nevada cave using ^{14}C and $^{87}Sr/^{86}Sr$. Geochim. Cosmochim. Acta 74, 5228–5242.
Paulsen, D.E., Li, H.-C., Ku, T.-L., 2003. Climate variability in central China over the last 1270 years revealed by high-resolution stalagmite records. Quat. Sci. Rev. 22, 691–701.
Pausata, F.S.R., Battisti, D.S., Nisancioglu, K.H., Bitz, C.M., 2011. Chinese stalagmite $\delta^{18}O$ controlled by changes in the Indian monsoon during a simulated Heinrich event. Nat. Geosci. 4, 474–480.
Pu, J.B., Wang, A.Y., Yin, J.J., Shen, L.C., Yuan, D.X., 2017. PCO_2 variations of cave air and cave water in a subtropical cave, SW China. Carbonates Evaporites 33, 477–487.
Riechelmann, D.F.C., Schröder-Ritzrau, A., Scholz, D., Fohlmeister, J., Spötl, C., Richter, D.K., Mangini, A., 2011. Monitoring Bunker Cave (NW Germany): a prerequisite to interpret geochemical proxy data of speleothems from this site. J. Hydrol. 409, 682–695.
Rudzka, D., McDermott, F., Baldini, L.M., Fleitmann, D., Moreno, A., Stoll, H., 2011. The coupled $\delta^{13}C$-radiocarbon systematics of three Late Glacial/early Holocene speleothems; insights into soil and cave processes at climatic transitions. Geochim. Cosmochim. Acta 75, 4321–4339.
Sherwin, C.M., Baldini, J.U.L., 2011. Cave air and hydrological controls on prior calcite precipitation and stalagmite growth rates: Implications for palaeoclimate reconstructions using speleothems. Geochim. Cosmochim. Acta 75, 3915–3929.
Shopov, Y., Stoykova, D., Tsankov, L., Sanabria, M., Georgieva, D., Ford, D., Georgiev, L., 2004. Influence of solar luminosity over geomagnetic and climatic cycles as derived from speleothems. Int. J. Speleol. 33, 19–24.
Spötl, C., Fairchild, I.J., Tooth, A.F., 2005. Cave air control on dripwater geochemistry, Obir Caves (Austria): Implications for speleothem deposition in dynamically ventilated caves. Geochim. Cosmochim. Acta 69, 2451–2468.

Staddon, P.L., 2004. Carbon isotopes in functional soil ecology. Trends Ecol. Evol. 19, 148–154.

Sun, Z., Yang, Y., Shi, Q., Zhang, P., Liang, S., Zhang, N., Liu, X., Nie, X.D., Peng, T., Liang, S.L., Zhang, Z.Q., 2017. Study on the influence factors of modern speleothem hiatus: a case from Jiguan Cave, Henan. Acta Sedimentologica Sinica 35 (1), 93-101 (in Chinese with English abstract).

Sun, Z., Yang, Y., Zhao, J.Y., Tian, N., Feng, X.X., 2018. Potential ENSO effects on the oxygen isotope composition of modern speleothems: Observations from Jiguan Cave, central China. J. Hydrol. 566, 164–174.

Tan, L.C., Cai, Y.J., Cheng, H., An, Z.S., Edwards, R.L., 2009. Summer monsoon precipitation variations in central China over the past 750years derived from a high-resolution absolute-dated stalagmite. Palaeogeogr. Palaeoclimatol. Palaeoecol. 280, 432–439.

Tan, L.C., Cai, Y.J., Cheng, H., Edwards, L.R., Lan, J.H., Zhang, H.W., Li, D., Ma, L., Zhao, P.P., Gao, Y.L., 2018. High resolution monsoon precipitation changes on southeastern Tibetan Plateau over the past 2300 years. Quat. Sci. Rev. 195, 122–132.

Tan, L.C., Dong, G.H., An, Z.S., Lawrence Edwards, R., Li, H.M., Li, D., Spengler, R., Cai, Y.J., Cheng, H., Lan, J.H., Orozbaev, R., Liu, R.L., Chen, J.H., Xu, H., Chen, F.H., 2020a. Megadrought and cultural exchange along the proto-silk road. Sci. Bull.

Tan, L.C., Liu, W., Wang, T.L., Cheng, P., Zang, J.J., Wang, X.Q., Ma, L., Li, D., Lan, J.H., Edwards, R.L., Cheng, H., Xu, H., Ai, L., Gao, Y.L., Cai, Y.J., 2020b. A multiple-proxy stalagmite record reveals historical deforestation in central Shandong, northern China. Sci. China Earth Sci. 63, 1622–1632.

Tan, L.C., Zhang, H.W., Qin, S.J., An, Z.S., 2013. Climatic and anthropogenic impacts on $\delta^{13}C$ variations in a stalagmite from Central China. Terrestrial, Atmospheric and Oceanic Sciences 24, 333.

Tan, M., 2014. Circulation effect: response of precipitation $\delta^{18}O$ to the ENSO cycle in monsoon regions of China. Clim. Dyn. 42, 1067–1077.

Tan, M., 2016. Circulation background of climate patterns in the past millennium: Uncertainty analysis and re-reconstruction of ENSO-like state. Sci. China Earth Sci. 59, 1225–1241.

Tooth, A.F., Fairchild, I.J., 2003. Soil and karst aquifer hydrological controls on the geochemical evolution of speleothem-forming drip waters, Crag Cave, southwest Ireland. J. Hydrol. 273, 51–68.

Treble, P.C., Bradley, C., Wood, A., Baker, A., Jex, C.N., Fairchild, I.J., Gagan, M.K., Cowley, J., Azcurra, C., 2013. An isotopic and modelling study of flow paths and storage in Quaternary calcarenite, SW Australia: implications for speleothem paleoclimate records. Quat. Sci. Rev. 64, 90–103.

Treble, P.C., Fairchild, I.J., Griffiths, A., Baker, A., Meredith, K.T., Wood, A., McGuire, E., 2015. Impacts of cave air ventilation and in-cave prior calcite precipitation on Golgotha Cave dripwater chemistry, southwest Australia. Quat. Sci. Rev. 127, 61–72.

Tremaine, D.M., Froelich, P.N., 2013. Speleothem trace element signatures: a hydrologic geochemical study of modern cave dripwaters and farmed calcite. Geochim. Cosmochim. Acta 121, 522–545.

Trumbore, S., 2000. Age of soil organic matter and soil respiration: Radiocarbon constraints on belowground C dynamics. Ecol. Appl. 10, 399–411.

Verheyden, S., Keppens, E., Fairchild, I.J., McDermott, F., Weis, D., 2000. Mg, Sr and Sr isotope geochemistry of a Belgian Holocene speleothem: implications for paleoclimate reconstructions. Chem. Geol. 169, 131–144.

Wang, Y.J., Cheng, H., Edwards, L.R., He, Y.Q., Kong, X.G., An, Z.S., Wu, J.Y., Kelly, M. J., Dykoski, C.A., Li, X.D., 2005. The Holocene Asian monsoon: links to solar changes and North Atlantic climate. Science 308, 854–857.

Wang, Y.J., Cheng, H., Edwards, R.L., An, Z.S., Wu, J.Y., Shen, C.C., Dorale, J.A., 2001. A high-resolution absolute-dated late Pleistocene Monsoon record from Hulu Cave, China. Science 294, 2345–2348.

Wei, K., Wang, Q.J., Zhou, B.B., He, B., 2017. Analysis of drought characteristic in Shaanxi province based on precipitation anomaly percentage. Soil Water Conservy 31, 318–322 (in Chinese with English abstract).

Wong, C.I., Banner, J.L., Musgrove, M., 2011. Seasonal dripwater Mg/Ca and Sr/Ca variations driven by cave ventilation: Implications for and modeling of speleothem paleoclimate records. Geochim. Cosmochim. Acta 75, 3514–3529.

Woo, K.S., Ji, H., Jo, K.-N., Yi, S., Cheng, H., Edwards, R.L., Hong, G.H., 2015. Reconstruction of the Northeast Asian monsoon climate history for the past 400 years based on textural, carbon and oxygen isotope record of a stalagmite from Yongcheon lava tube cave, Jeju Island, Korea. Quat. Int. 384, 37–51.

Wu, Y., Li, T.Y., Yu, T.L., Shen, C.C., Chen, C.J., Zhang, J., Li, J.Y., Wang, T., Huang, R., Xiao, S.Y., 2020. Variation of the Asian summer monsoon since the last glacial-interglacial recorded in a stalagmite from southwest China. Quat. Sci. Rev. 234, 106261.

Yuan, D.X., Hai, C., Edwards, R.L., Dykoski, C.A., Kelly, M.J., Zhang, M.L., Qing, J.M., Lin, Y.S., Wong, Y.J., Wu, J.Y., 2004. Timing, duration, and transitions of the last interglacial Asian monsoon. Science 304, 575–578.

Zhang, H.W., Cai, Y.J., Tan, L.C., Cheng, H., Qin, S.J., An, Z.S., Edwards, R.L., Ma, L., 2015. Large variations of $\delta^{13}C$ values in stalagmites from southeastern China during historical times: implications for anthropogenic deforestation. Boreas 44, 511–525.

Zhang, J., Li, T.Y., 2019. Seasonal and interannual variations of hydrochemical characteristics and stable isotopic compositions of drip waters in Furong Cave, southwest China based on 12 years' monitoring. J. Hydrol. 572, 40–50.

Zhang, P.Z., Cheng, H., Edwards, R.L., Chen, F.H., Wang, Y.J., Yang, X.L., Liu, J., Tan, M., Wang, X.F., Liu, J.H., An, C.L., Dai, Z.B., Zhou, J., Zhang, D.Z., Jia, J.H., Jin, L.Y., Johnson, K.R., 2008. A test of climate, sun, and culture relationships from an 1810-Year Chinese cave record. Science 322, 940–942.

Zhao, J.Y., Cheng, H., Yang, Y., Tan, L.C., Spötl, C., Ning, Y.F., Zhang, H.W., Cheng, X., Sun, Z., Li, X.L., Li, H.Y., Liu, W., Edwards, R.L., 2019. Reconstructing the western boundary variability of the Western Pacific Subtropical High over the past 200 years via Chinese cave oxygen isotope records. Clim. Dyn. 52, 3741–3757.

Zhao, M., Liu, Z.H., Li, H.C., Zeng, C., Yang, R., Chen, B., Yan, H., 2015. Response of dissolved inorganic carbon (DIC) and $\delta^{13}C_{DIC}$ to changes in climate and land cover in SW China karst catchments. Geochim. Cosmochim. Acta 165, 123–136.

Zheng, F., Zhu, J., 2015. Observed splitting eastbound propagation of subsurface warm water over the equatorial Pacific in early 2014. Sci. Bull. 60, 477–482.